Robotica (2018) volume 36, pp. 1627–1640. © Cambridge University Press 2018
doi:10.1017/S0263574718000607

Performance improvement of bilateral control systems using derivative of force

Eray A. Baran†*, Tarik Uzunovic‡ and Asif Sabanovic§

†*Faculty of Engineering and Natural Sciences, Istanbul Bilgi University, Istanbul, Turkey.*
‡*Faculty of Electrical Engineering, University of Sarajevo, Sarajevo, Bosnia and Herzegovina. E-mail: tuzunovic@etf.unsa.ba*
§*Faculty of Engineering and Natural Sciences, Sabanci University, Istanbul, Turkey. E-mail: asif@sabanciuniv.edu*

(Accepted June 30, 2018. First published online: July 30, 2018)

SUMMARY
This paper proposes a bilateral control structure with a realization of the force derivative in the control loop. Due to the inherent noisy nature of the force signal, most teleoperation schemes can make use of only a proportional (P) control structure in the force channel of the bilateral controllers. In the proposed scheme, an α–β–γ filter is designed to smoothly differentiate the force signal obtained from a reaction force observer integrated to both of the master and slave plants. The differentiated force signal is then used in a proportional-derivative (PD) force controller working together with a disturbance observer. In order to design the overall bilateral controller, an environment model based on pure spring structure is assumed. The controller is designed to enforce an exponentially decaying tracking error for both position and force signals. With the presented controller design approach, one can independently tune the controller gains of the force and the position control channels. The proposed approach is experimentally tested in a platform consisted of direct drive linear motors. As illustrated by the experiment results, the contribution of the PD control in the force channel improves the teleoperation performance especially under hard-contact motion scenarios by attenuating the oscillations, hence, improving the transparency when compared to the structures using only a P force control.

KEYWORDS: Haptics; Bilateral control; Teleoperation; PD force control; α–β–γ filter; Hard contact motion control.

1. Introduction

The scope of the applications requiring the ability of manipulation in a remote location has been increasing rapidly. In particular, semi-autonomous and risky tasks that require intervention of a human operator seek for solutions based on intermediate robotic systems to extend the manipulation ability. Bilateral control, as a method of teleoperation (i.e. operation at a distance), has thus been investigated by many researchers.[1–5] Among the potential applications of bilateral control, space robotics,[6,7] underwater explorations,[8] and robotic surgery systems[9–11] can be counted. In the most general sense, a teleoperation system contains two robots, namely, the master and the slave robots, mutually interacting with each other in order to match the force and position responses. The objective of a bilateral control algorithm is to enforce tracking of the master robot positions by the slave robot and reflection of the interaction forces of the slave robot back to the master robot. Simultaneous tracking of these forces and positions leads to an ideally desired situation called as transparent operation.[12] Under such an ideal operation, environmental impedance is fully transmitted to the human operator at the other end of the teleoperation system.

In the literature, several methods have been proposed to satisfy the goals of a teleoperation system. Early solutions were mainly concentrated on the elimination of the effect of time delay between

* Corresponding author. E-mail: eray.baran@bilgi.edu.tr

https://doi.org/10.1017/S0263574718000607 Published online by Cambridge University Press

the master and slave robots assuming a long distance operation. Among those solutions, Lyapunov-based controllers,[13] control schemes involving hybrid approaches,[14] and designs based on impedance representation[15] can be counted. The idea of using the scattering theory through network could improve the closed-loop dynamics by reducing the interference of wave reflections. Accordingly, controllers derived based on wave variables attained a good solution providing the stable operation with improved transparency under constant and known time delays.[16] Considering the nature of time delay between the master and slave robots, the two port time-domain passivity approach was modified to provide the stable teleoperation for systems with a time-varying delay. Perceiving the effect of the time delay as a disturbance acting on the teleoperation system, solutions based on the application of disturbance observers (DOBs) and model-based control were illustrated.[17] Analytical and quantitative comparison of some of the solutions for teleoperation systems can be found in refs. [18] and [19], respectively for continuous-time and discrete-time controllers.

Many researchers also focus on the problems of teleoperation systems for which signal transmission delays are not involved in the control loop[20,21] (i.e. systems targeting indoor operation). In that sense, one of the focus points is the scaling of the position and force responses of the master and slave robots as demanded in the teleoperation tasks between micro and macro systems.[22] An example of the studies addressing the scaling issue in bilateral control was presented in ref. [23], where the variable scaling is addressed. More recently, benefitting from the advances in the field of atomic force microscopy, researchers started to consider the perception of haptic feedback from the surfaces of nano structures through teleoperated robots.[24] Methodological evaluation of the performance in scaled teleoperation systems was investigated in ref. [25] considering the aspects of stability and transparency.

Regardless of the target application, bilateral control systems suffer from the inherent nature of the coupling between the force and position responses. In order to deal with that problem, some researchers proposed methods to better decompose the force and position loops.[4,26] The basic approach here is to use appropriate transformations to single out the force and position controllers so that they can be designed totally independently. The force and position signals are then matched in terms of the accelerations and are given as references to the acceleration controllable plants. In that approach, the overall performance of the bilateral control system depends on the independent controllers designed for position and force tracking. In majority of the bilateral control studies, the current state of the art relies on designing proportional-derivative (PD) and proportional (P) controllers for the position and the force control tasks, respectively.[27–31] Since the force signal has a very noisy characteristic, the derivative of the force (i.e. yank) cannot be effectively used in the control loop. Thus, even though the overall controller can provide certain level of transparency, the independent performance of the force control loop sets some limits. This problem was addressed in ref. [32] where an adaptive control approach was used to convert the teleoperation system into a rigid tool, applicable for both of the hard and soft contact motion scenarios. In that study, the implemented control system shows good performance in force tracking. However, the presented method is only valid within a pre-specified bandwidth, which limits the application range of the proposed algorithm. Another contribution to improve the force response was presented in ref. [33], where the non-linear friction force of the manipulators are subtracted from the operational force in order to improve the force control performance. Despite the relative improvements given in that study, the proposed method was not analyzed for applications considering rapid change of forces. Therefore, the attenuation of hard contact oscillations in the force control loop of the teleoperation systems still remain as a fundamental problem since the force control loops lack the damping term. On the other hand, using only a P control structure, the force control gains cannot be selected very high, which limits the bandwidth of the overall bilateral controller. Especially in hard contact situations where the force measurement changes very rapidly, a bilateral control system might show an oscillatory transient response, which reduces its application range.

This study is carried out to address the problem of pure P force control of bilateral teleoperation architectures and proposes a solution for the oscillatory behavior of the master and slave systems in hard contact motion. The proposed scheme builds on the decoupled controller design approach for the position and force control loops of a bilateral control system for which the time delays are negligibly small.[21] However, unlike the conventional methods, here, we propose the use of PD control for the force control task of the overall bilateral control system. In order to acquire a smooth yank signal, an α–β–γ tracker is realized and embedded to the force measurement channel. Furthermore, the design of the force control loop is reformulated in this paper using a spring dominated environment

https://doi.org/10.1017/S0263574718000607 Published online by Cambridge University Press

approach. The proposed controller is tested under extreme conditions in two sets of experiments and the responses are compared with the same bilateral control structure having only P control in the force channel. It is verified that the proposed bilateral controller performs very good, especially in hard contact environments, extending the application limits of the bilateral control theory.

The organization of the paper is as follows. Section 2 gives the background information for the general system definition, the acceleration control framework and the force estimation method used in this study. Section 3 presents the derivation of the bilateral controller showing independent design of the position and force controllers and their combination assuming a spring dominated environment model. In Section 4, the α–β–γ tracker-based smooth force differentiation is discussed. Section 5 illustrates the results of two independent sets of experiments and in Section 6, the concluding remarks are given.

2. Background Information

2.1. System definition

In the context of this study, derivation of the proposed control architecture is made assuming single degree of freedom (DOF) master and slave systems. Generalization of the presented scheme for multi-DOF systems can be possible once the necessary matrix algebra is carried out.[34] The equation of motion for a single DOF mechanical system can be given as

$$m(x)\ddot{x}(t) = f_r(t) - f_l(t), \tag{1}$$

where $m(x)$, $f_r(t)$, $f_l(t)$, and $x(t)$ represent the mass ⟨inertia⟩, the reference force ⟨torque⟩, the load force ⟨torque⟩, and the generalized coordinate of motion for a linear ⟨rotational⟩ system, respectively. The reference force exerted on the system can be taken as

$$f_r(t) = k_t i_r(t), \tag{2}$$

where k_t and $i_r(t)$ represent the actuator gain (i.e. the force constant) of the system under consideration and the reference current given to the system, respectively. For a single DOF freedom motion control system, the parameters $m(x)$ and k_t of Eqs. (1) and (2) may show variations (δm, δk) around their nominal values m_n and k_n, respectively, as

$$m(x) = m_n + \delta m, \tag{3}$$

$$k_t = k_n + \delta k. \tag{4}$$

In the light of this information, one can recast Eq. (1) as follows:

$$m_n\ddot{x}(t) = k_n i_r(t) - f_d(t). \tag{5}$$

The terms m_n, k_n, and $f_d(t)$ of (5), respectively, stand for the nominal mass of the system, nominal force constant of the system, and the disturbance force acting on the system. The content of the disturbance force $f_d(t)$ in (5) can be given as

$$f_d(t) = \delta m\ddot{x}(t) - \delta k i_r(t) + b(x, \dot{x})\dot{x} + g(x) + f_e(t). \tag{6}$$

In (6), terms $b(x, \dot{x})\dot{x}$, $g(x)$, and $f_e(t)$ represent the viscous friction force, gravitational force, and external force acting on the system. Terms $\delta m\ddot{x}(t)$ and $\delta k i_r(t)$ of the disturbance, on the other hand, stand for the acceleration induced force and the force due to the fluctuations of the force constant. The rest of the derivation will continue assuming the models given in (5) and (6).

2.2. Robust acceleration control with disturbance observer

In order to enforce the robust motion control on the system, rejection of the disturbance given in (6) is of particular importance. This can be accomplished via utilization of a DOB structure which makes

https://doi.org/10.1017/S0263574718000607 Published online by Cambridge University Press

use of the inverse nominal plant model and a low-pass filter to estimate the disturbance $\hat{f}_d(t)$ acting on the system. The basic principle and the structure of DOB used in the context of this study was given in ref. [35], while a more detailed study considering rapid changes of disturbance force was presented in ref. [36]. With the inclusion of DOB, the dynamics of the system can be restated as follows:

$$\ddot{x}(t) = \frac{k_n}{m_n} i_r(t) - \frac{\delta f_d(t)}{m_n}, \tag{7}$$

where $\delta f_d(t) \doteq f_d(t) - \hat{f}_d(t)$ is the remaining disturbance acting on the system. Since the division of the desired torque reference of the system by the nominal mass represents the desired acceleration ($\ddot{x}^{\text{des}}$) of the plant, one can further note the following identity:

$$\ddot{x}(t) = \ddot{x}^{\text{des}}(t) - \frac{\delta f_d(t)}{m_n}. \tag{8}$$

Equation (8) highlights an important aspect of systems with DOBs, since $\delta f_d(t) \ll f_d(t)$, a system with DOB can easily trace the desired acceleration references with a simple outer loop compensation such as a PD controller.[37] Based on this fact, in the following sections, derivation of the control input will follow a path to obtain the desired acceleration references using PD compensation.

2.3. Reaction force estimation

For the system under consideration, the acquisition of the reaction force information in a fast and accurate way plays an important role. This requirement can be fulfilled by a reaction force observer (RFOB) as illustrated in ref. [38].

The most critical issue for the accurate estimation of the reaction force is a precise identification of the system. Recalling Eq. (6), the external force is one of the components that add up to the total disturbance in the system. As the system has only single DOF, the fluctuations for the mass of the system are negligibly small (i.e. $m_n \gg \delta m \Rightarrow \delta m \approx 0$). On the other hand, current state-of-the-art in power electronics enable the production of very accurate drivers where the deviations of the force constant from its nominal value are very small (i.e. $k_n \gg \delta k \Rightarrow \delta k \approx 0$). Under these assumptions, the external force can be estimated as follows:

$$\hat{f}_e(t) = \hat{f}_d(t) - \tilde{b}(x, \dot{x})\dot{x} - \tilde{g}(x), \tag{9}$$

where $\tilde{b}(x, \dot{x})$ and $\tilde{g}(x)$ stand for the estimated viscous friction coefficient and the calculated gravitational force obtained after a parameter identification process and gathered from the system geometry, respectively. In refs. [39] and [40], it has been shown by the authors that the estimation of forces with an RFOB structure brings superior stability and performance improvement advantages over systems measuring the forces with sensors once a proper parameter identification is carried out. In the following sections, the derivation will follow the assumption that both of the master and the slave plants contain integrated DOB and RFOB to accomplish the robust acceleration control and accurate external force estimation.

2.4. Environment model

In order to formulate the force control loop of the bilateral controller, one has to identify the physical model of the environment interacted by either one of the master or slave systems. In the literature, there are several studies which model the mathematical base of the interaction force.[41,42] Among them, the most commonly used model is the standard contact impedance model as given in the following equation:

$$f_e = \delta m_e \ddot{x}_e + b_e \dot{x}_e + k_e \delta x_e. \tag{10}$$

In that model, the source of force generated during interaction depends on three main components, which are the inertial forces ($\delta m_e \ddot{x}_e$) that exist due to the acceleration of the mass that is displaced during motion, the viscous forces ($b_e \dot{x}_e$) due to the speed of motion in a resistive environment and the spring forces ($k_e \delta x_e$) due to the displacement of the environment from its original position. Having

https://doi.org/10.1017/S0263574718000607 Published online by Cambridge University Press

a more detailed look at these three components, one can observe the common relationship $\|k_e\| \gg \|b_e\| \gg \|\delta m_e\|$ between the displaced mass (δm_e), the damping coefficient (b_e), and the stiffness (k_e) for most of the physical systems.[43,44] In other words, a considerably high proportion of the interaction force is created by the stiffness of the environment. Another interpretation of this approximation is the possibility of disregarding the transient dynamics and focusing on the steady-state value of the interaction force during force control. Accordingly, in many studies concerning the robotic force control,[45,46] researchers take the environment model in its simplest form as follows:

$$f_e = k_e \delta x_e. \tag{11}$$

Here, $\delta x_e = x_* - x_e$ is the displacement of the environment position x_e by the system $*$ with respect to its original position. Assuming a stationary environment position, the relationship between the interaction force of system $*$ with the environment can be recast as

$$\dot{f}_* = k_e \dot{x}_*, \tag{12}$$

$$\ddot{f}_* = k_e \ddot{x}_*. \tag{13}$$

In the derivation given below, the force channel of the bilateral control algorithm is designed assuming that the interactions between the robots and the corresponding environments are governed by pure spring models as shown in (11). This assumption permits the realization of the PD force feedback in the expressions obtained for the desired acceleration, making it possible to use the PD force control in the system.

3. Derivation of Bilateral Controller

Referring back to Eq. (8) and recalling the fact that some estimation error remains, one can write the dynamics of the master and slave systems as

$$\ddot{x}_m(t) = \ddot{x}_m^{\text{des}}(t) - \frac{\delta f_{dm}(t)}{m_{nm}}, \tag{14}$$

$$\ddot{x}_s(t) = \ddot{x}_s^{\text{des}}(t) - \frac{\delta f_{ds}(t)}{m_{ns}}, \tag{15}$$

where additional subscripts m and s represent the master and the slave systems, respectively. Similarly, adopting the environment model given in (13), one can express the second-order dynamics of the interaction force for the master and slave systems as

$$\dddot{f}_m = k_{em} \ddot{x}_m, \tag{16}$$

$$\dddot{f}_s = k_{es} \ddot{x}_s. \tag{17}$$

Since the goals of a bilateral control system is to synchronize the positions and the interaction forces, one can define the following tracking errors:

$$e_p = x_m - x_s, \tag{18}$$

$$e_f = f_m + f_s, \tag{19}$$

where e_p and e_f, respectively, stand for the position and force tracking errors. The objective of the controller can then be expressed as enforcing the errors given in (18) and (19) tend to zero value. In order to fulfill this goal, the error vector $\mathbf{e}$ can now be defined as

$$\mathbf{e} = \begin{bmatrix} e_p \\ e_f \end{bmatrix}. \tag{20}$$

https://doi.org/10.1017/S0263574718000607 Published online by Cambridge University Press

Taking into account the identities given between (14) and (20), by proper substitutions the second-order dynamics of the error vector can be given as

$$\ddot{\mathbf{e}} = \begin{bmatrix} \ddot{e}_p \\ \ddot{e}_f \end{bmatrix} = \underbrace{\begin{bmatrix} 1 & -1 \\ k_{em} & k_{es} \end{bmatrix}}_{\mathbf{A}} \underbrace{\begin{bmatrix} \ddot{x}_m^{\text{des}} \\ \ddot{x}_s^{\text{des}} \end{bmatrix}}_{\ddot{\mathbf{x}}^{\text{des}}} - \underbrace{\begin{bmatrix} \frac{\delta f_{dm}}{m_{nm}} - \frac{\delta f_{ds}}{m_{ns}} \\ k_{em}\frac{\delta f_{dm}}{m_{nm}} - k_{es}\frac{\delta f_{ds}}{m_{ns}} \end{bmatrix}}_{\mathbf{d}}. \tag{21}$$

Without loss of generality, one can select the desired accelerations for the master and slave device using error feedback with PD control as follows:

$$\ddot{\mathbf{x}}^{\text{des}} = \mathbf{A}^{-1}\left(-\mathbf{W}\dot{\mathbf{e}} - \mathbf{Y}\mathbf{e}\right), \tag{22}$$

where $\mathbf{W}$ and $\mathbf{Y}$ are diagonal matrices with positive diagonal entries:

$$\mathbf{W} = \begin{bmatrix} w_1 & 0 \\ 0 & w_2 \end{bmatrix}, \; w_1, w_2 > 0, \tag{23}$$

$$\mathbf{Y} = \begin{bmatrix} y_1 & 0 \\ 0 & y_2 \end{bmatrix}, \; y_1, y_2 > 0. \tag{24}$$

Substituting (22) back to the desired accelerations in (21), the dynamics of the vector $\mathbf{e}$ takes the following form:

$$\ddot{\mathbf{e}} + \mathbf{W}\dot{\mathbf{e}} + \mathbf{Y}\mathbf{e} = -\mathbf{d}. \tag{25}$$

From (25), it can be concluded that the error vector has stable dynamics, and the disturbance estimation errors influence only at the steady-state position and force errors, through the vector $\mathbf{d}$. If satisfactory disturbance compensations exist at the master and the slave sides, one can assume that both components of the vector $\mathbf{d}$ are very small and thus $\|\mathbf{d}\| \xrightarrow{t\to\infty} 0$. Hence, with proper disturbance compensation, the resulting dynamics of the error vector can be written as

$$\ddot{\mathbf{e}} + \mathbf{W}\dot{\mathbf{e}} + \mathbf{Y}\mathbf{e} = \mathbf{0}. \tag{26}$$

The content of Eq. (26) can be rewritten in the form

$$\ddot{e}_p + w_1\dot{e}_p + y_1 e_p = 0, \tag{27}$$

$$\ddot{e}_f + w_2\dot{e}_f + y_2 e_f = 0. \tag{28}$$

Here, selecting $w_1 = r_{p1} + r_{p2} > 0$, $y_1 = r_{p1}r_{p2} > 0$, $w_2 = r_{f1} + r_{f2} > 0$, and $y_2 = r_{f1}r_{f2} > 0$ with r_{pi} and r_{fi}, respectively, standing for the ith root of the Eqs. (27) and (28), one can enforce the exponential convergence of the position and force errors to zero without overshoots:

$$e_p \xrightarrow{t\to\infty} 0, \tag{29}$$

$$e_f \xrightarrow{t\to\infty} 0. \tag{30}$$

Here, it can be highlighted that one can also enforce different dynamics of the position error and force error by selecting elements of the matrices $\mathbf{W}$ and $\mathbf{Y}$. In other words, the control gains for the position and force channels can be independently tuned without affecting the dynamics of each other.

Implementation of the control algorithm (22) requires the derivatives of the interaction forces f_m and f_s as it appears in $\dot{\mathbf{e}}$. In the next section, acquisition of the force derivative signal will be discussed. In order to obtain the coefficients of the proposed controller, one can rearrange (22) and show the

https://doi.org/10.1017/S0263574718000607 Published online by Cambridge University Press

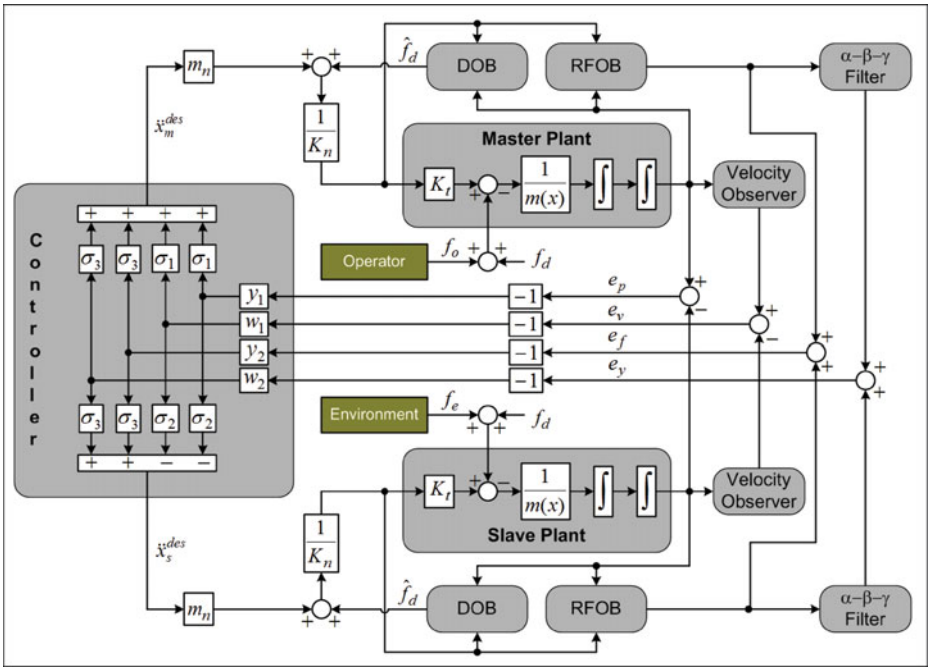

Fig. 1. Schematic representation of the proposed controller.

desired acceleration matrix as

$$\begin{bmatrix} \dddot{x}_m^{\text{des}} \\ \dddot{x}_s^{\text{des}} \end{bmatrix} = \frac{1}{k_{es}+k_{em}} \begin{bmatrix} k_{es} & 1 \\ -k_{em} & 1 \end{bmatrix} \begin{bmatrix} -w_1 e_v - y_1 e_p \\ -w_2 e_y - y_2 e_f \end{bmatrix}, \tag{31}$$

where e_p, e_v, e_f, and e_y stand for the position, velocity, force, and yank (i.e. the derivative of force) errors, respectively. The identity given in (31) can be expanded and the explicit expressions for the desired accelerations of the master and the slave systems can be acquired by defining parameters $\eta = \frac{k_{es}}{k_{em}}$, $\sigma_1 = \frac{\eta}{\eta+1}$, $\sigma_2 = \frac{1}{\eta+1}$, and $\sigma_3 = \frac{1}{k_{es}+k_{em}}$ as follows:

$$\dddot{x}_m^{\text{des}} = -\sigma_1 w_1 e_v - \sigma_1 y_1 e_p - \sigma_3 w_2 e_y - \sigma_3 y_2 e_f, \tag{32}$$

$$\dddot{x}_s^{\text{des}} = \sigma_2 w_1 e_v + \sigma_2 y_1 e_p - \sigma_3 w_2 e_y - \sigma_3 y_2 e_f. \tag{33}$$

Equations (32) and (33), once given on acceleration controllable plants, enforce the master and slave systems accomplish the tracking objectives given in (18) and (19). Besides the controller gains w_1, w_2, y_1, and y_2, parameters σ_1, σ_2, and σ_3 provide further flexibility in controller design. Recalling that $\eta = \frac{k_{es}}{k_{em}}$, one can analyze the effect of gains σ_i, $i \in \{1, 2, 3\}$ based on the possible configurations of the master and the slave environments. If the slave environment is much harder than that of the master environment (i.e. $k_{es} \gg k_{em}$), the gains can be arranged as $\sigma_1 \approx 1$ and $\sigma_2 \approx 0$. On the other hand, for applications where the slave environment is much softer than the master environment (i.e. $k_{es} \ll k_{em}$), one can select these gains as $\sigma_1 \approx 0$ and $\sigma_2 \approx 1$. For unknown environments, one can either take $\sigma_1 = \sigma_2 = 0.5$ or realize an adaptive structure for the estimation and updating of these parameters. Such an adaptive structure, however, is beyond the scope of this paper.

It is important to discuss here the advantage brought by the design approach presented above. The vector sitting on the right side of the expression shown in (31) indicates that the position and force loops contain decoupled PD controllers. The contribution of that structure is the ability to single out these two loops and tune the corresponding controller coefficients independently. Hence, the user is equipped with the tools to adjust the error convergence rates of the position and the force loops without interfering with the dynamics of one another. For better understanding of the controller structure, a block diagram showing the overall signal flow of the proposed scheme is shown in Fig. 1.

https://doi.org/10.1017/S0263574718000607 Published online by Cambridge University Press

4. Smooth Force Differentiation with α–β–γ Filter

The acquisition of the smooth derivative of the force signal is a serious problem since a straightforward differentiation results in a highly deteriorated response where signal to noise ratio (SNR) is very low. As also proposed in this study, the use of yank (i.e. the derivative of force) in the control loop requires a fast and clear differentiation of the reaction force. In order to attain this goal, the force response obtained from RFOB is passed through an α–β–γ filter. The preference of α–β–γ structure over the standard α–β tracker is due to its ability to track the accelerating targets with zero steady-state error.[47] Below, a brief overview of α–β–γ filter is presented without the details of derivation. The same set of equations are summarized in ref. [48] where the filter is further extended to α–β–γ–δ structure which is applicable for third-order systems. For interested readers, refs. [49] and [50] provide further detailed information about the α–β–γ filter.

Without loss of generality, one can assume the following state evolution for the signal to be differentiated:

$$q_p[k+1] = q_h[k] + T\dot{q}_h[k] + \frac{1}{2}T^2\ddot{q}_h[k], \tag{34}$$

$$\dot{q}_p[k+1] = \dot{q}_h[k] + T\ddot{q}_h[k], \tag{35}$$

$$\ddot{q}_p[k+1] = \ddot{q}_h[k], \tag{36}$$

where q is the system state to be differentiated and T is the sampling period of the discrete-time algorithm. In (34)–(36), the subscripts $*_p$ and $*_h$ represent the predicted and smoothed values of the corresponding state $*$, respectively. The innovation of the smoothed states based on the measured values are then given by

$$q_h[k] = q_p[k] + \alpha\left(q_o[k] - q_p[k]\right), \tag{37}$$

$$\dot{q}_h[k] = \dot{q}_p[k] + \frac{\beta}{T}\left(q_o[k] - q_p[k]\right), \tag{38}$$

$$\ddot{q}_h[k] = \ddot{q}_p[k] + \frac{\gamma}{2T^2}\left(q_o[k] - q_p[k]\right), \tag{39}$$

where the variable $q_o[k]$ stand for the measured state. The selection of the values for parameters α, β, and γ identify the characteristics of the filter being used. Having a stable tracking of the original signal and its derivatives requires the following boundaries for these parameters as obtained from the Jury's stability analysis:[48]

$$0 < \alpha < 2, \tag{40}$$

$$0 < \beta < (4 - 2\alpha), \tag{41}$$

$$0 < \gamma < \tfrac{4\alpha\beta}{(2-\alpha)}. \tag{42}$$

In order to illustrate the performance of α–β–γ filter for the acquisition of the yank signal, a simulation is done and the results are shown in Fig. 2. In the simulation, a motion control system is manipulated with an arbitrary reference, forcing it to interact with an artificial environment. The position reference of the system in the simulation is corrupted with white noise and the force measurement is made using an RFOB. Within the control loop, the measured force is differentiated in two different ways: one being the backward Euler differentiation with a third-order low-pass filter and the other being obtained from an α–β–γ filter. The third-order low-pass filter for the backward Euler differentiation is specifically selected to have a better evaluation of the responses since the α–β–γ filter itself has third-order characteristics. The parameters for the simulation under consideration are, respectively, selected to be $\alpha = 0.5$, $\beta = 0.0005$, and $\gamma = 0.000002$ using trial and error, while the cut-off frequency of the third-order low-pass filter used in the backward Euler differentiation is adjusted to $\omega_c = 159$ rad/s (i.e. ≈ 1000 Hz).

The results of the force response, the yank response obtained by backward Euler differentiation and the yank response obtained by α–β–γ filter-based differentiation are shown in Fig. 2(A)–(C),

https://doi.org/10.1017/S0263574718000607 Published online by Cambridge University Press

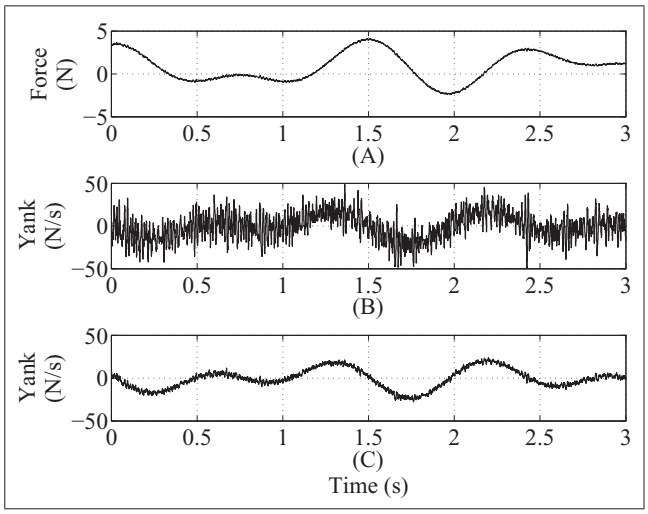

Fig. 2. Simulation results of force differentiation: Force response (A), backward Euler differentiation of force with third-order low-pass filter (B), differentiation of force with α–β–γ filter (C).

respectively. As obvious from the given plots, the α–β–γ filter can give a much smoother response than that of the standard differentiation methods. In order to quantify the difference between these two approaches, the SNR for the two yank signals are calculated using the following formula:

$$\mathrm{SNR}(\mathbf{w}) = \frac{\sqrt{\frac{1}{L}\sum_{i=1}^{L} u_i^2}}{\sqrt{\frac{1}{L}\sum_{i=1}^{L} n_i^2}}, \tag{43}$$

where $\mathbf{w}$, $\mathbf{u}$, $\mathbf{n}$, and L stand for the noisy signal, the actual (noise-free) signal, the noise on the actual signal (i.e. $\mathbf{w} = \mathbf{u} + \mathbf{n}$), and the length of the data set, respectively. The calculated SNR values are 1.428 and 6.849 for the backward Euler differentiated signal and the α–β–γ filter-based differentiated signal, respectively.

5. Experiments

In order to validate the proposed teleoperation architecture, two sets of experiments are carried out. In the first experiment set, the master system is controlled by another single DOF system, physically connected to the master robot. The goal in this experiment is to give the same motion reference to the master system and observe the responses of the bilateral control architectures with pure P force control and PD force control. In both of these architectures, the controller gains are pushed to the limits and slave system is enforced to have hard contact.

In the second set of experiments, the master robot is manipulated by a human operator with arbitrary motion references and the slave robot is interacted with a very hard environment. The goal in this experiment is to highlight the extent of the proposed control architecture. In order to better illustrate the performance of the controller, in this experiment the slave robot is used as a hammer to insert nail on a piece of wood which is remotely operated by the reference enforced on the master robot. The configuration of the experimental setup for these two experiments are explained in the following subsection.

5.1. Experimental platform

The first group of experiments are made on a platform consisted of three systems standing for the master robot, the slave robot, and the operator robot which generates the same motion profile for the master robot in both experiments (i.e. ones with P and PD force control loops). All three robots contain a Faulhaber LM2070 series direct drive linear motor equipped with an appropriate driver and a Renishaw RGH41 series encoder which has 500 nm resolution. Real-time operation of the algorithm

https://doi.org/10.1017/S0263574718000607 Published online by Cambridge University Press

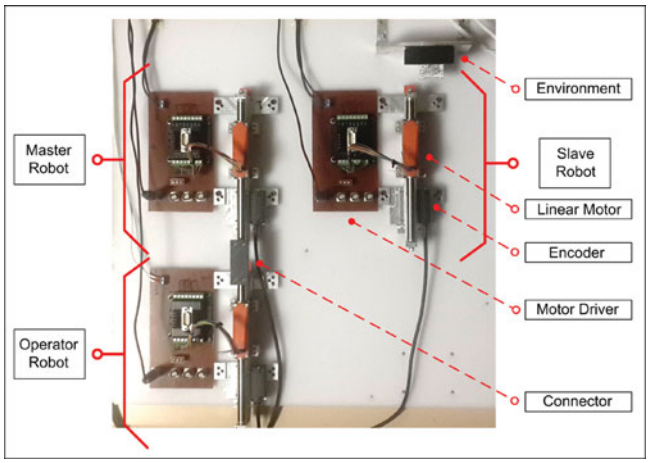

Fig. 3. Configuration of the experimental platform for the computer generated uniform references.

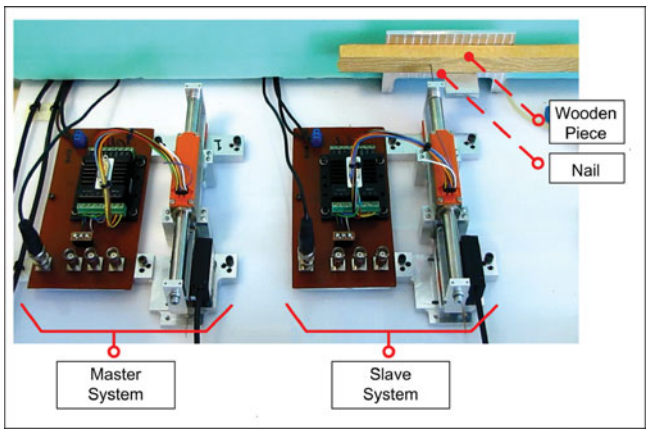

Fig. 4. Configuration of the experimental platform for random references generated by a human operator.

is realized in a DSpace DS1103 system running at 10 KHz loop execution frequency. The depiction of the setup used in the first experiment set is given in Fig. 3.

The second experiment set is made on a setup with a similar configuration. In the second setup, however, the master robot is rearranged to be free (i.e. the operator robot is removed from the system) such that a human operator can generate the motion reference of the master robot. In order to validate the performance of the proposed architecture, the second experiment is tested on various hard and soft contact scenarios. For better illustration purposes, however, the results taken during penetration with a hard environment is given here in the experiment results section. The setup used in the second experiment is shown in Fig. 4.

In both of the experiment configurations, the same set of control and filtering parameters are used. The decision on the values of these parameters are made after extensive trial and error. During the tuning process, first, low values are selected for these parameters and then the selected values are increased to the limits after which there is no further improvement in the results. The parameters used in the experiments are summarized in Table I.

5.2. Experimental results

The results obtained from two different sets of experiments are presented in Figs. 5 and 6 for the uniform (i.e. the robot operator) and the random (i.e. the human operator) master motion references, respectively. In the first experiment, the operator robot is controlled to apply a constant 5.8 N force on the master robot and the slave robot strikes a steel environment positioned at 0.03 m. Looking at the responses illustrated in Fig. 5(C) and (D), the oscillations in the force response are considerably

https://doi.org/10.1017/S0263574718000607 Published online by Cambridge University Press

Table I. Parameters used in the experiments for controller and filter.

Parameter	Value	Parameter	Value
y_1	3000	η	0.5
w_1	200	α	0.5
y_2	75	β	0.0005
w_2	5	γ	0.000002

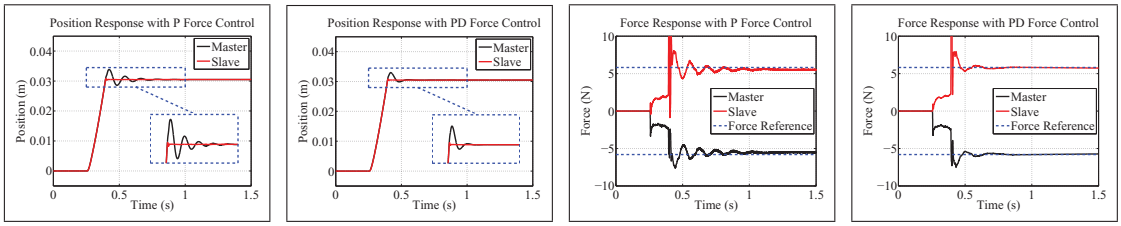

(A) (B) (C) (D)

Fig. 5. Comparison of the bilateral controller responses with P control and PD control in the force channel under the uniform reference motion: Position responses (A)–(B), force responses (C)–(D).

less in PD controller than that of the conventional P controller. The settling times for the responses are 0.76 s and 0.33 s, respectively, for P and PD force controllers. Another salient feature of the force responses is the steady-state error. The steady state errors of the controllers are 5.17% for the conventional controller and 1.21% for the proposed controller. On the other hand, due to the nature of the haptic interaction, the improvement on the force response is also reflected in the position tracking performance as shown in Fig. 5(A) and (B). The overshoots in position response are reduced from 11.2% to 8.2% in the proposed controller structure.

In the second experiment set, on the other hand, the response and the tracking error of the proposed controller are illustrated when a human operator manipulates the master robot. The operator uses the master robot as a hammer for the first 5 s to insert a nail on a wooden piece located at 0.05 m position. After 5 s, the operator continues to push the master robot, while the slave system preserves the contact with the nail. The hard contact responses can be observed from the peaks in Fig. 6(C) and (D). In order to better evaluate the proposed controller, the errors between the master and the slave system responses with respect to the corresponding references for the

- free motion without contact,
- moment of the hard contact, and
- motion in contact with the environment

are evaluated independently in terms of the peak and mean values. The peak and the mean values of the percentage errors are given in Table II. The values shown in the table indicate mean percentage errors of less than 1% and peak percentage errors of less than 4% for both of the free motion and the motion in contact. On the other hand, the error values at the moment of hard contact are bigger as expected. This is because of the rapid change of the slave system velocity during the hard contact. Since actuator's maximum force cannot stop the master system (i.e. the master motor's force limit is achieved), the error between the two systems rise temporarily. However, even in that hard contact moment with such errors, the controller preserves stability and successfully eliminates the error with a very short transient.

6. Conclusion

This study presents a DOB-based acceleration controller structure for the decoupled force and position controller design of a teleoperation system. Unlike the other existing studies, the paper proposes the use of the force derivative in the control loop of the bilateral control system. Replacing the conventional

https://doi.org/10.1017/S0263574718000607 Published online by Cambridge University Press

Table II. Percentage tracking errors.

Free motion (no contact)		
Response	Peak error	Mean error
Position	0.49%	0.04%
Velocity	2.19%	0.22%
Force	3.45%	0.41%
Yank	1.39%	0.22%
Hard contact moment		
Response	Peak error	Mean error
Position	1.77%	0.59%
Velocity	42.66%	28.26%
Force	21.23%	17.70%
Yank	25.76%	21.91%
Motion in contact		
Response	Peak error	Mean error
Position	0.49%	0.21%
Velocity	2.24%	0.61%
Force	0.33%	0.06%
Yank	0.39%	0.06%

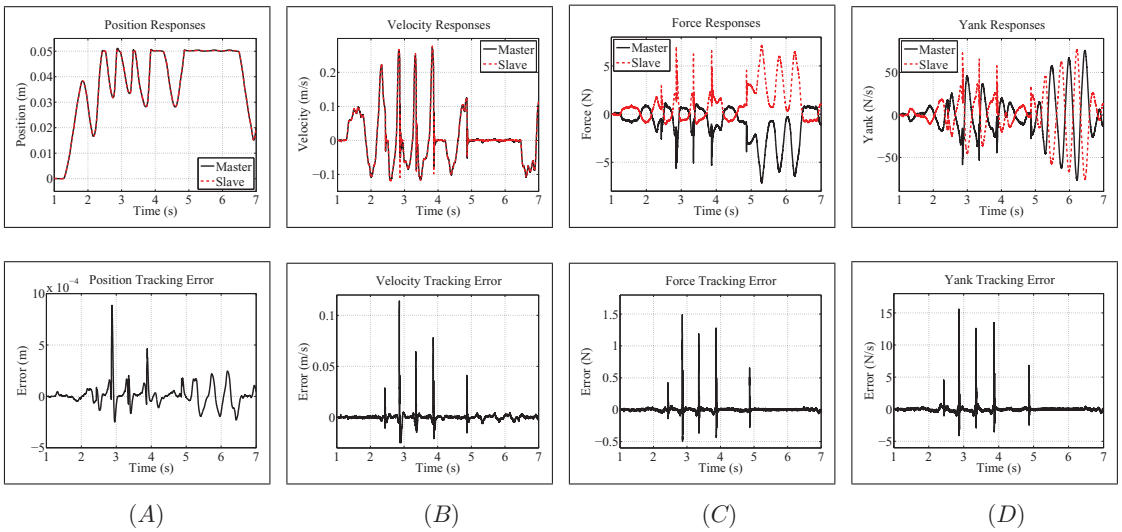

Fig. 6. Master and slave tracking responses and errors under random free and contact motion by a human operator. Position response and error (A). Velocity response and error (B). Force response and error (C). Yank response and error (D).

P control structure with a PD controller, the controller gains in the force channel are increased. Higher control gains and derivative action in the force channel eventually improve the overall teleoperation performance via decreasing the hard contact oscillations and providing a more stable, transparent, and vivid operation capability. The proposed controller structure is tested on two different sets of experiments both of which include extreme hard contacts with the environment. Preserving stable operation under the hard contact situations, the master-slave system can be used under very harsh conditions (e.g. even as a hammer to insert a nail on a piece of wood at a remote location). The results of the experiments show the promising contribution with the inclusion of the force derivative in the bilateral control which is prone to opening new paradigms in teleoperation controller design.

https://doi.org/10.1017/S0263574718000607 Published online by Cambridge University Press

Acknowledgments
The authors would like to acknowledge Tubitak Projects 114M578 and 110M425 and the Ministry of Civil Affairs of Bosnia and Herzegovina, for the partial support provided for this study.

Supplementary Material
To view supplementary material for this article, please visit https://doi.org/10.1017/S0263574718000607.

References

1. A. Hace and M. Franc, "Pseudo-sensorless high-performance bilateral teleoperation by sliding-mode control and FPGA," *IEEE/ASME Trans. Mechatronics* **19**(1), 384–393 (2014).
2. C. Mitsantisuk, K. Ohishi and S. Katsura, "Estimation of action/reaction forces for the bilateral control using Kalman filter," *IEEE Trans. Ind. Electron.* **59**(11), 4383–4393 (2012).
3. T. Mizoguchi, T. Nozaki and K. Ohnishi, "Stiffness transmission of scaling bilateral control system by gyrator element integration," *IEEE Trans. Ind. Electron.* **61**(2), 1033–1043 (2014).
4. S. Sakaino, T. Sato and K. Ohnishi, "Multi-DOF micro-macro bilateral controller using oblique coordinate control," *IEEE Trans. Ind. Electron.* **7**(3), 446–454 (2011).
5. S. Katsura, W. Yamanouchi and Y. Yokokura, "Real-world haptics: Reproduction of human motion," *IEEE Ind. Electron. Mag.* **6**(1), 25–31 (2012).
6. M. Wilde, Z. K. Chua and A. Fleischner, "Effects of multivantage point systems on the teleoperation of spacecraft docking," *IEEE Trans. Human-Mach. Syst.* **44**(2), 200–210 (2014).
7. E. Stoll, J. Letschnik, U. Walter, J. Artigas, P. Kremer, C. Preusche and G. Hirzinger, "On-orbit servicing," *IEEE Robot. Autom. Mag.* **16**(4), 29–33 (2009).
8. R. Saltaren, R. Aracil, C. Alvarez, E. Yime and J. M. Sabater, "Field and service applications-exploring deep sea by teleoperated robot-an underwater parallel robot with high navigation capabilities," *IEEE Robot. Autom. Mag.* **14**(3), 65–75 (2007).
9. F. Ferraguti, N. Preda, A. Manurung, M. Bonfe, O. Lambercy, R. Gassert, R. Muradore, P. Fiorini and C. Secchi, "An energy tank-based interactive control architecture for autonomous and teleoperated robotic surgery," *IEEE Trans. Robot.* **31**(5), 1073–1088 (2015).
10. J. Burgner, D. C. Rucker, H. B. Gilbert, P. J. Swaney, P. T. Russell, K. D. Weaver and R. J. Webster, "A telerobotic system for transnasal surgery," *IEEE/ASME Trans. Mechatron.* **19**(3), 996–1006 (2014).
11. H. Tanaka, K. Ohnishi, H. Nishi, T. Kawai, Y. Morikawa, S. Ozawa and T. Furukawa, "Implementation of bilateral control system based on acceleration control using Fpga for multi-DOF haptic endoscopic surgery robot," *IEEE Trans. Ind. Electron.* **56**(3), 618–627 (2009).
12. D. A. Lawrence, "Stability and transparency in bilateral teleoperation," *IEEE Trans. Robot. Autom.* **9**(5), 624–637 (1993).
13. F. Miyazaki, S. Matsubayash, T. Yoshimi and S. Arimoto, "A New Control Methodology Toward Advanced Teleoperation of Master-Slave Robot Systems," *Proceedings of the IEEE International Conference on Robotics and Automation*, vol. 3 (1986) pp. 997–1002.
14. B. Hannaford and P. Fiorini, "A Detailed Model of Bi-Lateral Teleoperation," *Proceedings of the IEEE International Conference on Systems, Man and Cybernetics* (1988)
15. G. J. Raju, G. C. Verghese and T. B. Sheridan, "Design Issues In 2-Port Network Models of Bilateral Remote Manipulation," *Proceedings of the IEEE International Conference on Robotics and Automation* (1989) pp. 1316–1321.
16. G. Niemeyer and J. J. E. Slotine, "Stable adaptive teleoperation," *IEEE J. Ocean. Eng.* **16**(1), 152–162 (1991).
17. K. Natori, T. Tsuji, K. Ohnishi, A. Hace and K. Jezernik, "Time delay compensation by communication disturbance observer for bilateral teleoperation under time-varying delay," *IEEE Trans. Ind. Electron.* **57**(3), 1050–1062 (2010).
18. G. Sankaranarayanan and B. Hannaford, "Experimental Comparison of Internet Haptic Collaboration with Time-Delay Compensation Techniques," *Proceedings of the IEEE International Conference on Robotics and Automation* (2008) pp. 206–211.
19. A. A. Ghavifekr, A. R. Ghiasi and M. A. Badamchizadeh, "Discrete-time control of bilateral teleoperation systems: A review," *Robotica* **36**(4), 552–569 (2018).
20. T. Nozaki, T. Mizoguchi, Y. Saito, T. Nakano and K. Ohnishi, "Bilateral control method based on transformation matrix relating motion features and tool coordinates," *IEEJ J. Ind. Appl.* **2**(1), 67–73 (2013).
21. S. Yajima and S. Katsura, "Decoupled bilateral control based on modal space observer in master-slave systems with different masses," *Electr. Eng. Japan* **193**(1), 10–20 (2015).
22. K. Ogawa, R. Kozuki and K. Ohnishi, "A Method for Improving Scaling Bilateral Control by Integration of Physical and Control Scaling Ratio," *Proceedings of the IEEE International Conference on Mechatronics* (2015) pp. 516–521.

https://doi.org/10.1017/S0263574718000607 Published online by Cambridge University Press

23. E. V. Poorten, T. Kanno and Y. Yokokohji, "Robust Variable-Scale Bilateral Control for Micro Teleoperation" *Proceedings of the IEEE International Conference on Robotics and Automation* (2008) pp. 655–662.
24. C. D. Onal and M. Sitti, "Teleoperated 3-D force feedback from the nanoscale with an atomic force microscope," *IEEE Trans. Nanotechnol.* **9**(1), 46–54 (2010).
25. S. E. Salcudean, S. Ku and G. Bell, "Performance Measurement in Scaled Teleoperation for Microsurgery," *CVRMed-MRCAS'97*, Springer (1997) pp. 789–798.
26. S. Sakaino, T. Sato and K. Ohnishi, "Oblique Coordinate Control for Advanced Motion Control-Applied to Micro-Macro Bilateral Control," *Proceedings of the IEEE International Conference on Mechatronics* (2009) pp. 1–6.
27. T. Nozaki, T. Mizoguchi and K. Ohnishi, "Decoupling strategy for position and force control based on modal space disturbance observer," *IEEE Trans. Ind. Electron.* **61**(2), 1022–1032 (2014).
28. J. Rebelo, T. Sednaoui, E. B. den Exter, T. Krueger and A. Schiele, "Bilateral robot teleoperation: A wearable arm exoskeleton featuring an intuitive user interface," *IEEE Robot. Autom. Mag.* **4**(21), 62–69 (2014).
29. S. B. Kesner and R. D. Howe, "Robotic catheter cardiac ablation combining ultrasound guidance and force control," *Int. J. Robot. Res.* **33**(4), 631–644 (2014).
30. B. Yang, S. Roys, U. X. Tan, M. Philip, H. Richard, R. P. Gullapalli and J. P. Desai, "Design, development and evaluation of a master slave surgical system for breast biopsy under continuous MRI," *Int. J. Robot. Res.* **33**(4), 616–630 (2014).
31. A. Suzumura and Y. Fujimoto, "Generalized design of position-based bilateral control parameterized by complementary sensitivity function," *IEEE Trans. Ind. Electron.* **65**(11), 8707–8717 (2018).
32. W. H. Zhu and S. E. Salcudean, "Stability guaranteed teleoperation: An adaptive motion/force control approach," *IEEE Trans. Autom. Control* **45**(11), 1951–1969 (2000).
33. K. Seki, S. Fujihara and M. Iwasaki, "Improvement of force transmission performance considering nonlinear friction in bilateral control systems," *IFAC-PapersOnLine* **50**(1), 12071–12076 (2017).
34. S. M. Shahruz, "Active vibration suppression in multi-degree-of-freedom systems by disturbance observers," *J. Viber. Control* **15**(8), 1207–1228 (2009).
35. K. Ohnishi, M. Shibata and T. Murakami, "Motion control for advanced mechatronics," *IEEE/ASME Trans. Mechatron.* **1**(1), 56–67 (1996).
36. C. O. Saglam, E. Baran, A. O. Nergiz and A. Sabanovic, "Model Following Control with Discrete Time SMC for Time-Delayed Bilateral Control Systems," *Proceedings of the IEEE International Conference on Mechatronics* (2011) pp. 997–1002.
37. M. J. Kim and W. K. Chung, "Disturbance-observer-based PD control of flexiblel joint robots for asymptotic convergence," *IEEE Trans. Robot.* **31**(6), 1508–1516 (2015).
38. T. Murakami, F. Yu and K. Ohnishi, "Torque sensorless control in multidegree-of-freedom manipulator," *IEEE Trans. Ind. Electron.* **40**(2), 259–265 (1993).
39. E. Sariyildiz and K. Ohnishi, "On the explicit robust force control via disturbance observer," *IEEE Trans. Ind. Electron.* **62**(3), 1581–1589 (2015).
40. E. Sariyildiz and K. Ohnishi, "A Comparison Study for Force Sensor and Reaction Force Observer Based Robust Force Control Systems," *Proceedings of the IEEE International Symposium on Industrial Electronics* (2014) pp. 1156–1161.
41. D. Erickson, M. Weber and I. Sharf, "Contact stiffness and damping estimation for robotic systems," *Int. J. Robot. Res.* **22**(1), 41–57 (2003).
42. M. H. Araghi and S. P. Salisbury, "Improved evaluation of dynamic mechanical properties of soft materials with applications to minimally invasive surgery," *IEEE/ASME Trans. Mechatron.* **18**(3), 973–980 (2013).
43. C. Mitsantisuk, K. Ohishi and S. Katsura, "Variable Mechanical Stiffness Control Based on Human Stiffness Estimation," *Proceedings of the IEEE International Conference on Mechatronics* (2011) pp. 731–736.
44. T. Tsumugiwa, R. Yokogawa and K. Hara, "Variable Impedance Control Based on Estimation of Human Arm Stiffness for Human-Robot Cooperative Calligraphic Task," *Proceedings of the IEEE International Conference on Robotics and Automation* (2002) pp. 644–650.
45. Z. Yang, A. Poo and G. Hong, "A New Method for Implementing Active Stiffness Control of Robot Manipulator by Using Sliding Mode," *Proceedings of the Asia-Pacific Workshop on Advances in Motion Control* (1993) pp. 165–170.
46. S. Chiaverini, B. Siciliano and L. Villani, "A survey of robot interaction control schemes with experimental comparison," *IEEE/ASME Trans. Mechatron.* **4**(3), 273–285 (1999).
47. Z. Han and S. Li, "Bp-Neural Network Alpha-Beta-Gamma Filter Optimized by GA," *Proceedings of the IEEE Conference on Industrial Electronics and Applications* (2009) pp. 1952–1956.
48. C. M. Wu, P. P. Lin, Z. Y. Han and S. R. Li, "Simulation-based optimal design of α–β–γ–δ filter," *Int. J. Automat. Comput.* **7**(2), 247–253 (2010).
49. W. Blair, "Two-Stage Alpha-Beta-Gamma Estimator for Tracking Maneuvering Targets," *Proceedings of the American Control Conference* (1992) pp. 842–846.
50. D. F. Crouse, "A general solution to optimal fixed-gain (–etc.) filters," *IEEE Signal Process. Lett.* **22**(7), 901–904 (2015).

https://doi.org/10.1017/S0263574718000607 Published online by Cambridge University Press